Supplementary Information

Ostwald ripening-induced hollow photoactive Zn-MOFs-confined electron-deficient Cu NPs for enhanced photocatalytic oxidative dehydrogenation to quinoline

Leixin Hou,[a]* Yanli Chen,[a] Ziyan Li,[a] Congfa Bian,[a] Youyi Li,[a] Mi Zhang,[a] Guilin Wen,[a] Daofu Liu[a] and Huilin Huang[b]*

[a] School of Chemistry and Materials Engineering, Huainan Normal University, Huainan, Anhui, 232000, P. R. China

[b] School of Chemical and Printing Dyeing Engineering, Henan University of Engineering, Zhengzhou, 451191, P. R. China

Corresponding Authors

* E-mail: houleixin@hnnu.edu.cn, huanghuilin321@126.com

Contents

1. General Materials and Methods
2. Synthesis and Characterization of Photocatalysts
3. Experimental Details for Oxidative Dehydrogenation of THQ Derivatives Mediated by Cu/Zn-TPBD
4. References

1. General Materials and Methods

All starting chemicals and reagents were commercially available and used without further purification unless specifically mentioned. H_4TPBD were synthesized following the literature procedures without modification.[S1]

Powder X-ray diffraction (PXRD) patterns were collected on a Bruker D2 PHASER diffractometer using Cu Kα radiation (λ = 1.54056 Å). Thermogravimetric (TG) analyses were carried out on a TGA5500 thermoanalyzer with a heating rate of 10 °C·min^{-1} under N_2 flow (100 mL·min^{-1}) from room temperature to 800 °C. The Nitrogen adsorption-desorption isotherms were determined at 77 K using a Quantachrome Autosorb iQZ apparatus. The specific surface areas were evaluated by the Brunauer-Emmett-Teller (BET) method. The Zn and Cu concentrations of Cu/Zn-TPBD were quantified by inductively coupled plasma-optical emission spectrometry (ICP-OES) (Agilent 700 Series). The scanning electron microscope (SEM) images were acquired using the ZEISS SIGMA 300 SEM. Transmission electron microscopy (TEM) images were recorded using a JEM-2200FS TEM instrument. Fourier transform infrared (FT-IR) measurements were performed on an Avatar 370 FT-IR spectrometer using KBr pellets. Raman spectra were collected on a Lab Raman HR Evolution at excitation wavelength of 633 nm in a scan range from 500 to 2200 cm^{-1}. X-ray photoelectron spectroscopy (XPS) was measured using Thermo ESCALAB-250XI. Femtosecond (1 to 1500 ps) transient absorption (fs-TAS) experiments were carried out using transient absorption pump–probe detection systems (HELIOS FIRE and EOS, Ultrafast Systems). Liquid UV–vis spectra were performed on a TU-1900 spectrophotometer. Solid-state UV-Vis DRS were collected on a UV-3600 UV-vis-NIR spectrophotometer with $BaSO_4$ as the reference. Photoluminescence spectra were obtained on a high-resolution FLS980 spectrofluorometer. The Electron paramagnetic resonance (EPR) spectra were acquired at room temperature under ambient conditions using a JEOL JES-FA200 spectrometer. ^{1}H NMR spectra were recorded in the designated solvents on Bruker AVANCEIII 400 M spectrometer with chemical shift in ppm.

2. Synthesis and Characterization of Photocatalysts

Synthesis of Zn-TPBD

The Zn-TPBD was synthesized with modifications according to our previous report literature.[S2] Typically, 0.3 g of $Zn(NO_3)_2{\cdot}4H_2O$, 0.1 g of H_4TPBD, and 5 mg of cetylammonium bromide (CTAB), 15 mL of dimethylacetamide (DMAc), and 5 mL of MeOH were ultrasonically mixed in a 50 mL Teflon-lined tube. The Teflon-lined tube was put into an autoclave and heated in an oven at 105 °C for 12 h and subsequently cooled to room temperature. The bright yellow product was collected by centrifugation, washed with DMF and acetone three times. After solvent exchange with acetone, the activated Zr-TPBD was dried at 60 °C under vacuum for overnight.

Synthesis of Cu/Zn-TPBD

50 mg of $Cu(NO_3)_2{\cdot}3H_2O$ and 20 mg of activated Zn-TPBD were dispersed into 15 mL of DMF and 5 mL of ethylene glycol (EG) via continuous sonication for 30 min. Then, the above mixture solution was transferred to a 50 mL Teflon-lined stainless autoclave and heated at 150 °C for 2 days. After the reaction, the products were collected by centrifugation, washed thoroughly with DMF and ethanol and finally dried under vacuum at 60 °C for 12 h. The powder was obtained as Cu/Zn-TPBD. For comparison, by adjusting $Cu(NO_3)_2{\cdot}3H_2O$ feeding to 20, 30 and 40 mg, the controlled samples with Cu contents of 1.2, 3.5 and 7.8 wt% were synthesized, denoted as Cu_1/Zn-TPBD (1.2%), Cu_1/Zn-TPBD (3.5%) and Cu_1/Zn-TPBD (7.8%), respectively.

The proposed mechanism for Cu nanoparticle reduction and formation during the Cu/Zn-TPBD synthesis process involves: (1) coordination: upon ultrasonic dispersion of $Cu(NO_3)_2$ in DMF and EG, Cu^{2+} coordinates with Zn-TPBD's oxygen containing groups, forming stable metal–organic complexes. (2) reduction: at high temperatures, Zn-TPBD's amino/unsaturated C=C bonds oxidize, releasing electrons to reduce Cu^{2+} to Cu^0. Concurrently, DMF decomposes, generating reductants (H_2O, NH_3) that enhance Cu^{2+} reduction. (3) nucleation: the reduced Cu^0 preferentially nucleates at specific Zn-TPBD's porous/coordination sites, which template ordered Cu nanoparticle arrangement.[S3-S5]

Photoelectrochemical Measurements

The photoelectrochemical characterization was performed utilizing a CHI 760E workstation (Chenhua Instruments, Shanghai, China) equipped with a standard three-electrode system, including an indium tin oxide (ITO) deposited with samples as the working electrode, an Ag/AgCl (KCl saturated) reference electrode and a Pt counter electrode. Typically, the photocatalyst material (5 mg) was fully ultrasonically dispersed in a mixed solution comprising 10 μL of 5 wt% Nafion, 4.0 mL of ethanol, and 1.0 mL of deionized water to form uniformly turbid liquid. Then, the suspension was drip-coated onto a 1 × 1 cm^2 ITO glass substrate to ensure that the active area of the catalyst was approximately 1 cm^2. At last, the obtained work electrode was dried at room temperature. A 0.5 M Na_2SO_4 aqueous solution was employed as the electrolyte for the photocurrent tests while the aqueous solution of 0.5 M KCl and 0.05 M $K_3[Fe(CN)_6]/K_4[Fe(CN)_6]$ was employed as the electrolyte for the EIS measurements. In the photocurrent tests, a 300 W Xe lamp (cut 420 nm) was used as a light source. For EIS measurements, the samples were tested with a frequency range from 10 kHz to 0.1 Hz. Mott-Schottky experimental plots were determined at frequencies of 500, 1000, and 1500 Hz.

XAFS Analysis

The Cu K-edge XAFS spectra measurements were conducted at the beamline 14W1 station in Shanghai Synchrotron Radiation Facility, operated at 3.5 GeV with a maximum electron current of 250 mA. X-ray was monochromatized by a Si (111) double crystal monochromator with the energy calibrated using a standard Cu foils. The acquired EXAFS data were performed and analyzed according to the standard procedures using the Athena module in the IFEFFIT software packages.[S6] The k^3-weighted EXAFS spectra were obtained by first removing the post-edge background from the total absorption and then normalized it relative to the edge-jump step. Afterward, the k^3-weighted χ(k) data were Fourier transformed into real (R) space using a Hanning window (d_K = 1.0 $Å^{-1}$) to distinguish the EXAFS contributions from various coordination shells.

General Procedure of Oxidative Dehydrogenation of Tetrahydroquinoline and Derivatives

Typically, 5 mg of the photocatalyst, 0.1 mmol of 1,2,3,4-tetrahydroquinoline and derivatives, and 10 mL of acetonitrile as the solvent were added to a quartz reactor after dispersing evenly by ultrasonic vibration. Subsequently, the quartz reactor was bubbled with O_2 for 30 min to remove the air and then sealed with an O_2 balloon with a pressure of about 1 atm. Then, the mixture was magnetically stirred at 1000 rpm and simultaneously irradiated by a 450 nm LED light source. The temperature was controlled by circulating water and maintained at 25 °C for the reaction. After the reaction was completed for 12 h, the reaction mixture was taken out and centrifuged at 9000 rpm to remove the solid photocatalyst, and the filtrate was concentrated under vacuum. The residue was then subjected to column chromatography on silica gel to afford the final dehydrogenation compounds.

Recycling Experiments

For the recycling study, the photocatalysts were collected through centrifugation after the reaction, washed with acetonitrile (3 × 5 mL), and dried in an oven at 80 °C overnight for use in the next run under the optimum reaction conditions.

Radical Inhibition Experiments

To identify the active intermediates during the photocatalytic process, radical scavenging experiments were carried out by adding different radical scavengers including *p*-benzoquinone (*p*-BQ), triethylenediamine (DABCO), $AgNO_3$, KI, and isopropanol (IPA), which were employed to scavenge superoxide radicals ($^{\bullet}O_2^-$), singlet oxygen ($^1O_2$), electrons (e^-), holes (h^+) and hydroxyl radicals (·OH), respectively. The photocatalytic experiments in the presence of scavengers were carried out under identical conditions.

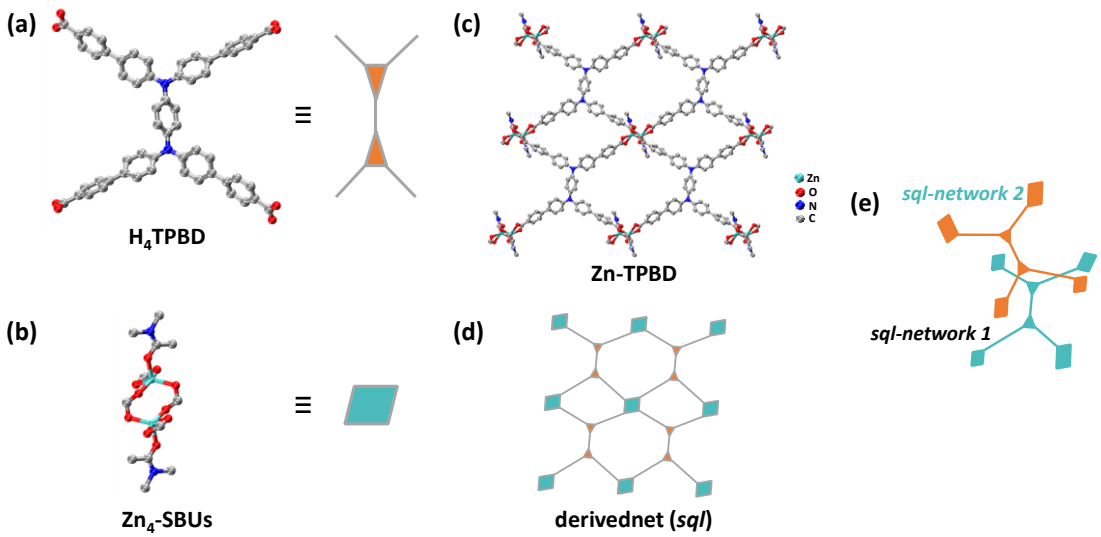

Figure S1. Structure description of (a) H_4TPBD organic linker and (b) zinc-containing SBUs. (c) Portion of two-dimensional structure of Zn-TPBD. Color scheme: zinc, cyan; oxygen, red; nitrogen, blue; fluorine, green; carbon, silver. (d) Underlying network derived from sql topology. (e) Interpenetration of the two sql networks along the crystallographic b-axis.

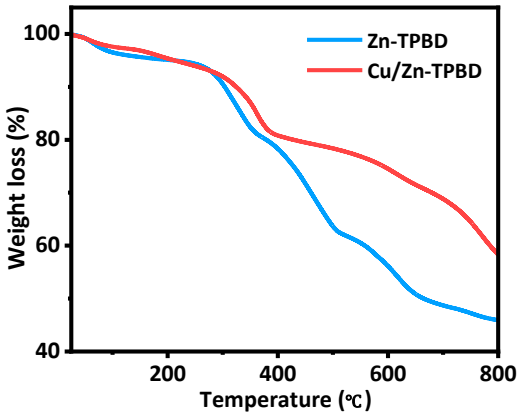

Figure S2. TGA curves of Zn-TPBD and Cu/Zn-TPBD.

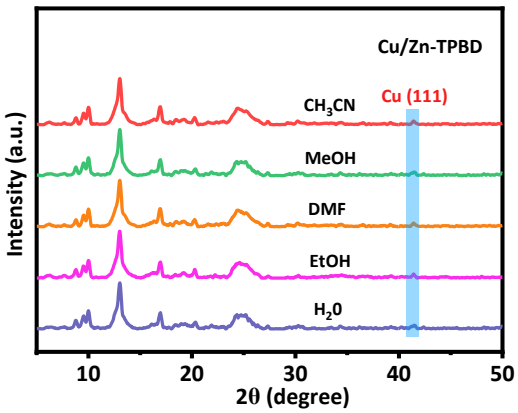

Figure S3. PXRD patterns of Cu/Zn-TPBD in different solvents.

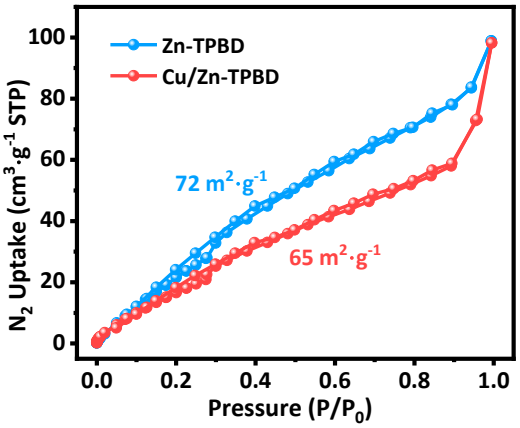

Figure S4. N_2 adsorption-desorption isotherms of Zn-TPBD and Cu/Zn-TPBD.

Table S1. Elemental analyses of Cu/Zn-TPBD sample.

Sample	Atomic contents				
	C (wt %)	N (wt %)	O (wt %)	Zn (wt %)	Cu (wt %)
Cu/Zn-TPBD	50.5	4.6	20.3	15.4	9.2
Cu_1/Zn-TPBD (7.8%)	49.9	4.7	21.2	16.5	7.8
Cu_1/Zn-TPBD (3.5%)	51.7	4.9	22.5	17.4	3.5
Cu_1/Zn-TPBD (1.2%)	52.2	4.8	23.2	18.6	1.2

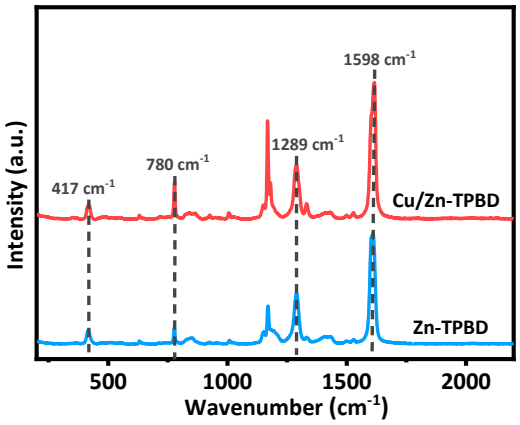

Figure S5. The laser Raman confocal microspectrometry of Zn-TPBD and Cu/Zn-TPBD.

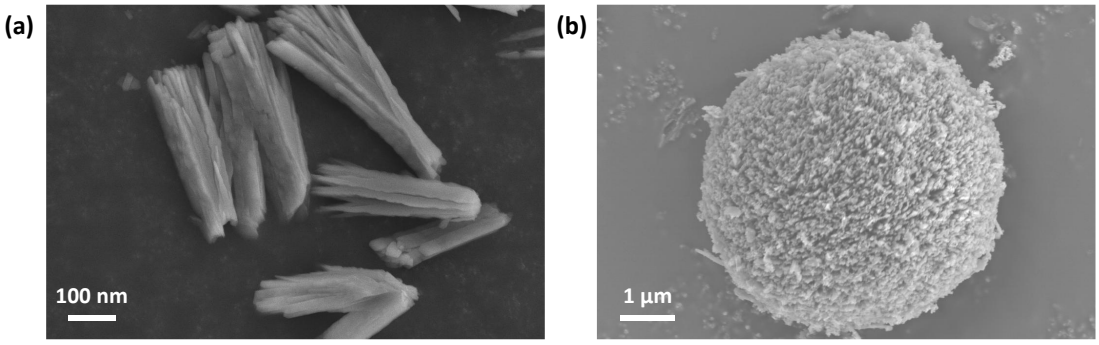

Figure S6. SEM images of (a) Zn-TPBD and (b) Cu/Zn-TPBD.

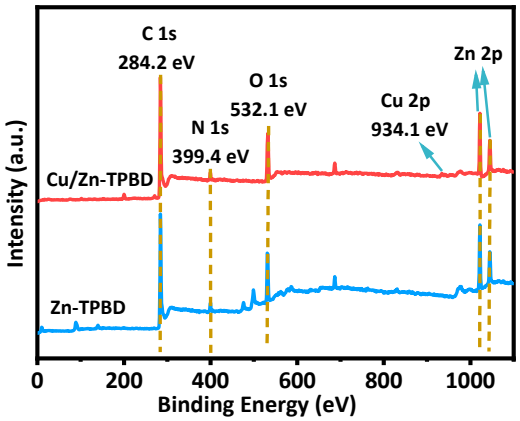

Figure S7. XPS full-scale spectrum of Zn-TPBD and Cu/Zn-TPBD.

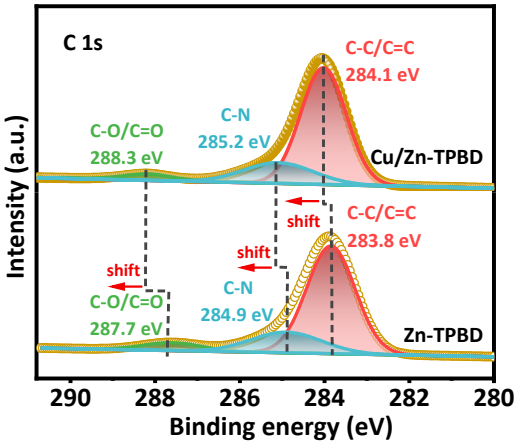

Figure S8. C1s spectrum of Zn-TPBD and Cu/Zn-TPBD.

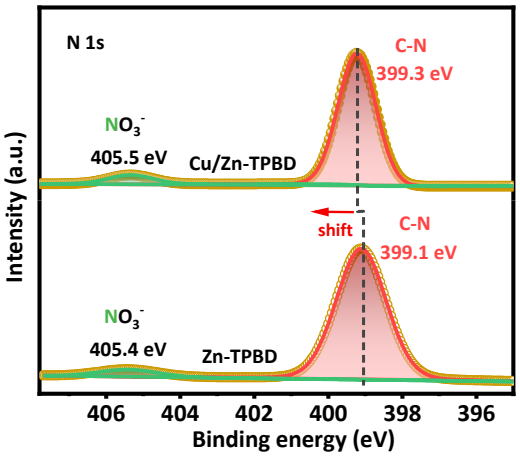

Figure S9. N1s spectrum of Zn-TPBD and Cu/Zn-TPBD.

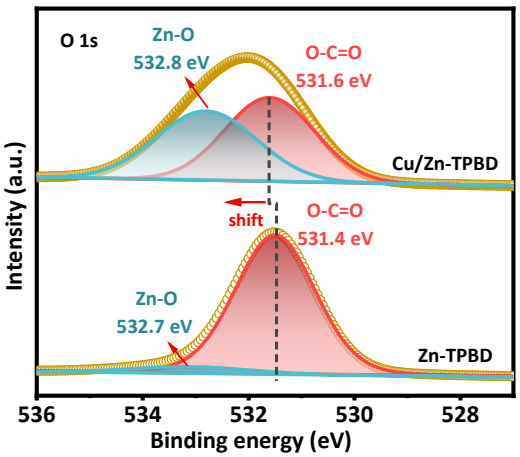

Figure S10. O1s spectrum of Zn-TPBD and Cu/Zn-TPBD.

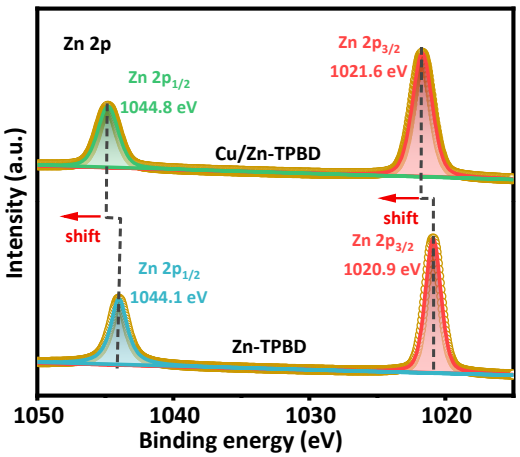

Figure S11. Zn*2p* spectrum of Zn-TPBD and Cu/Zn-TPBD.

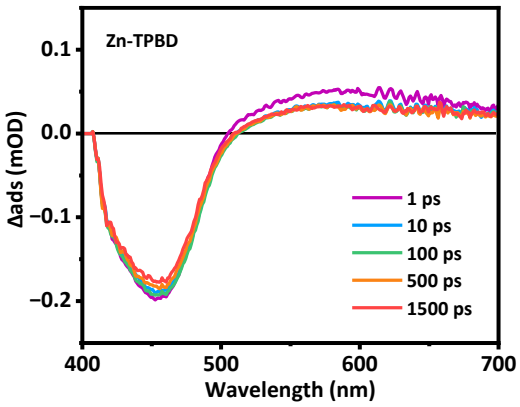

Figure S12. Transient absorption spectra recorded for Zn-TPBD upon pumping at 450 nm at different delay times.

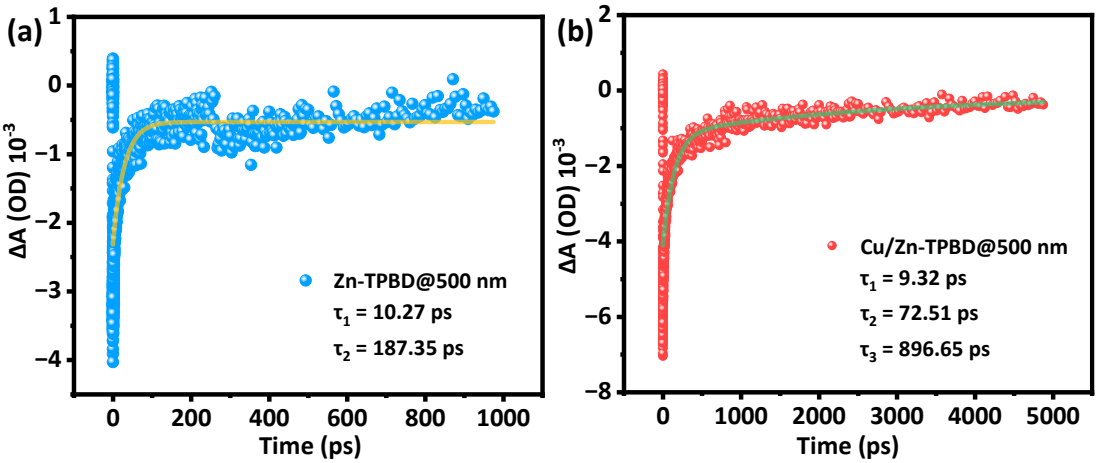

Figure S13. Decay kinetic curves of (a) Zn-TPBD and (b) Cu/Zn-TPBD.

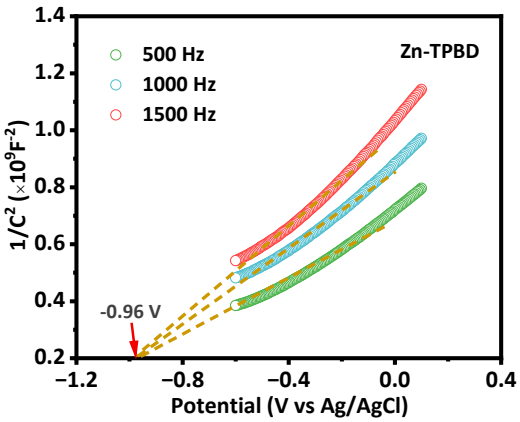

Figure S14. Mott-Schottky plots of Zn-TPBD.

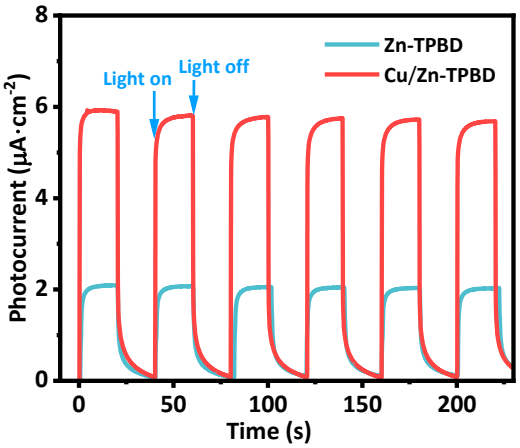

Figure S15. Transient photocurrent responses of Zn-TPBD and Cu/Zn-TPBD.

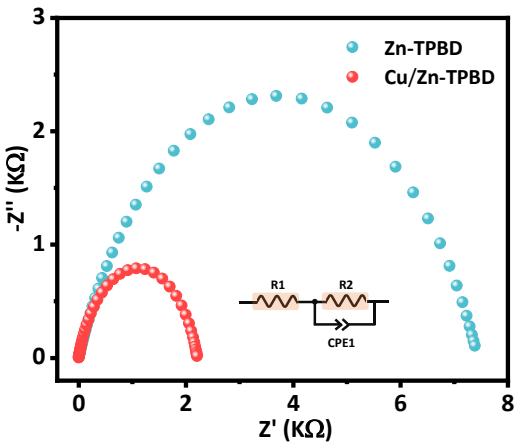

Figure S16. EIS Nyquist plots of Zn-TPBD and Cu/Zn-TPBD.

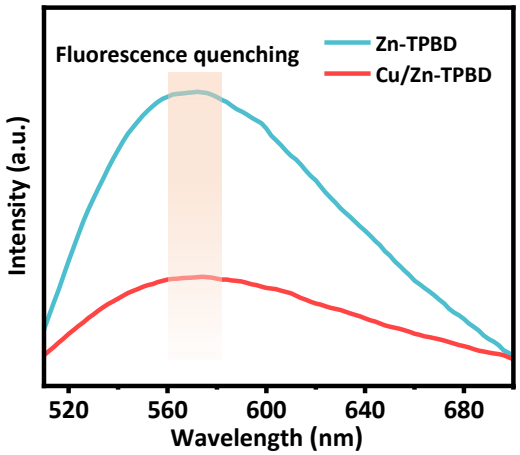

Figure S17. Solid-state luminescence spectra of Zn-TPBD and Cu/Zn-TPBD.

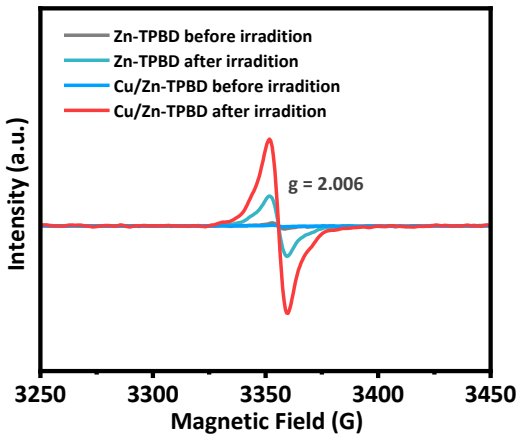

Figure S18. EPR spectra for Zn-TPBD and Cu/Zn-TPBD before and after light illumination for 5 min.

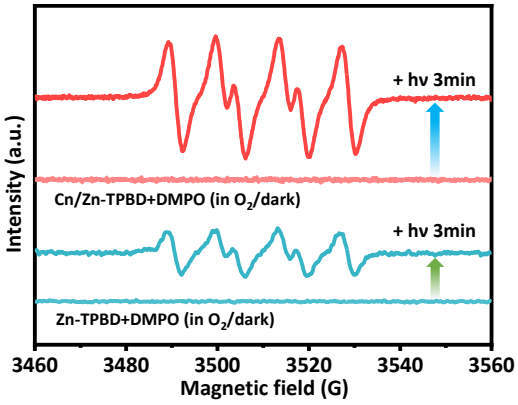

Figure S19. Comparative EPR detection of the dark and upon visible light irradiation of Zn-TPBD and Cu/Zn-TPBD with DMPO in presence of O_2.

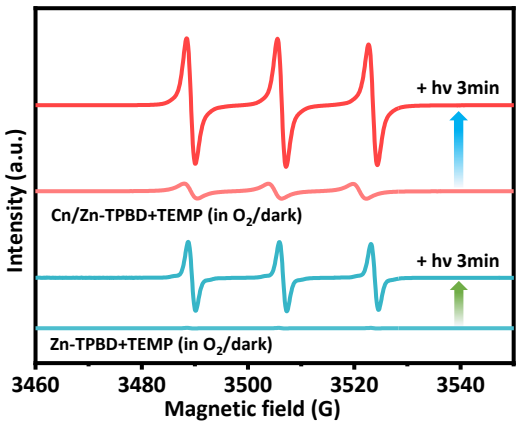

Figure S20. Comparative EPR detection of the dark and upon visible light irradiation of Zn-TPBD and Cu/Zn-TPBD with TEMP in presence of O_2.

3. Experimental Details for Oxidative Dehydrogenation of THQ Derivatives Mediated by Cu/Zn-TPBD

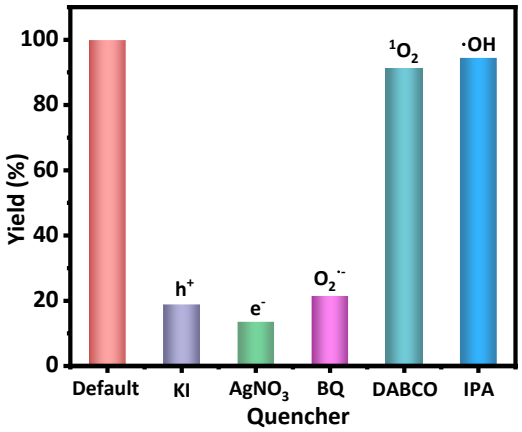

Figure S21. Effect of scavengers on the oxidative dehydrogenation reactions of 1,2,3,4-tetrahydroquinoline catalyzed by Cu/Zn-TPBD.

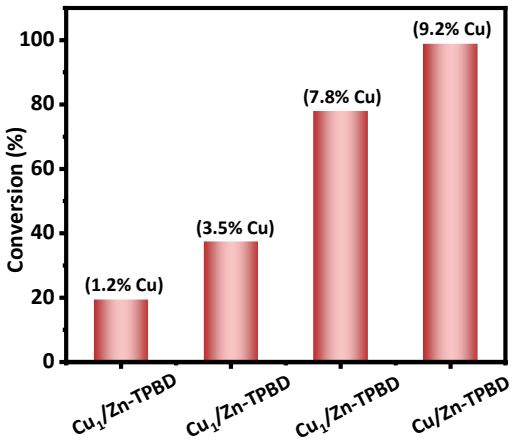

Figure S22. Yields of oxidative dehydrogenation of 1,2,3,4-tetrahydroquinoline using Cu/Zn-TPBD with varying Cu loadings under visible-light irradiation.

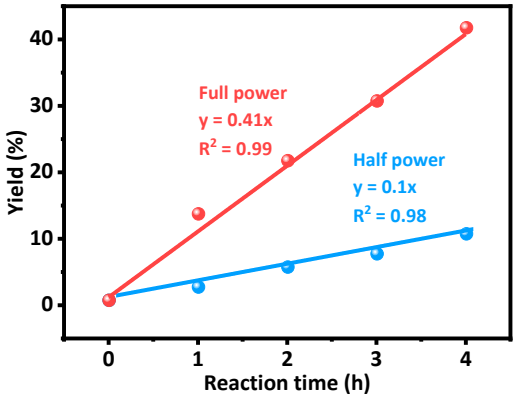

Figure S23. The oxidative dehydrogenation reaction yields of THQ as a function of the time under the standard conditions with a 450 nm LED irradiation of full power and half power within 4 hours, respectively.

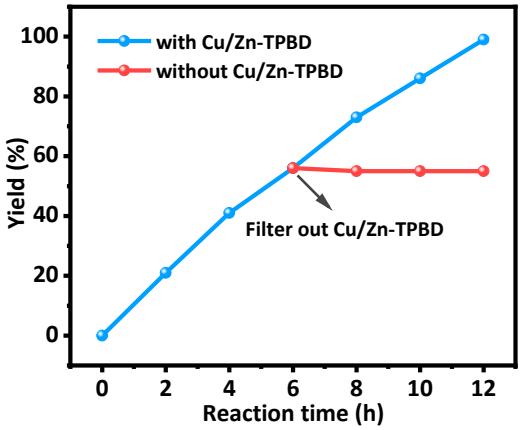

Figure S24. Catalyst filtration test for the oxidative dehydrogenation reactions of 1,2,3,4-tetrahydroquinoline catalyzed by Cu/Zn-TPBD.

The production of H_2O_2 was analyzed by the well-established iodimetry method. Typically, 0.5 mL 0.4 mol·L^{-1} potassium iodide (KI) solution and 0.5 mL 0.1 mol L^{-1} potassium hydrogen phthalate ($C_8H_5KO_4$) solution were added to 0.05 mL of obtained reaction supernatant by centrifugation and kept for 30 min. The H_2O_2 molecules sufficiently reacted with iodide anions (I^-) under acidic conditions ($H_2O_2 + 3I^- + 2H^+ \rightarrow I_3^- + 2H_2O$) to form triiodide anions (I_3^-) possessing a strong absorption at around 350 nm. The content of I_3^- was determined by measuring the absorbance at 350 nm by UV–vis spectroscopy, from which the total amount of H_2O_2 produced during each reaction can be calculated.

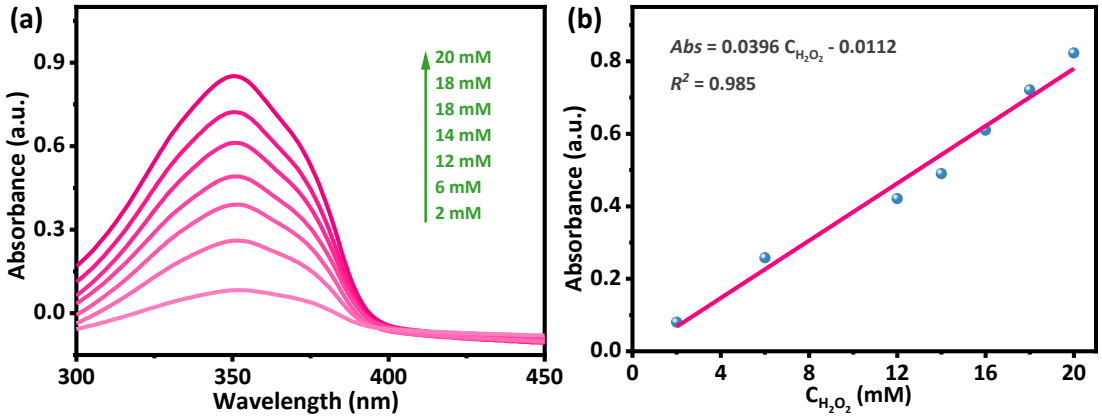

Figure S25. (a) UV-Vis absorption spectra of different H_2O_2 concentrations by iodimetry. (b) The standard linear relationship between the absorption and H_2O_2 concentrations.

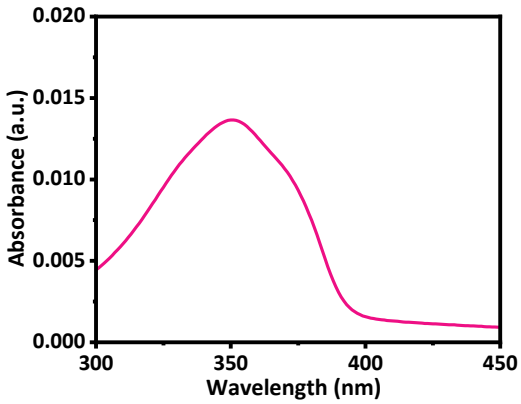

Figure S26. UV-Vis spectrum of H_2O_2 generation in the reaction solution after 12 hours of Cu/Zn-TPBD photooxidative dehydrogenation of 1,2,3,4-tetrahydroquinoline.

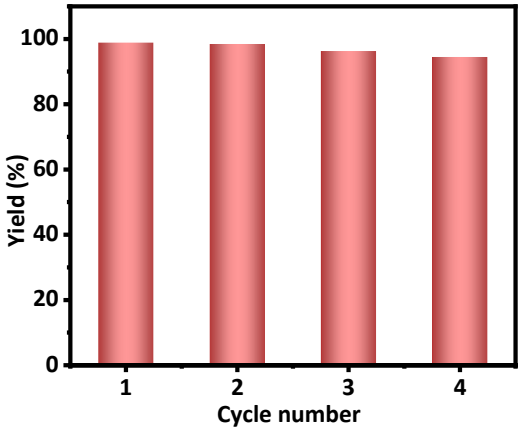

Figure S27. Yields of oxidative dehydrogenation of 1,2,3,4-tetrahydroquinoline using Cu/Zn-TPBD recycled from the reaction.

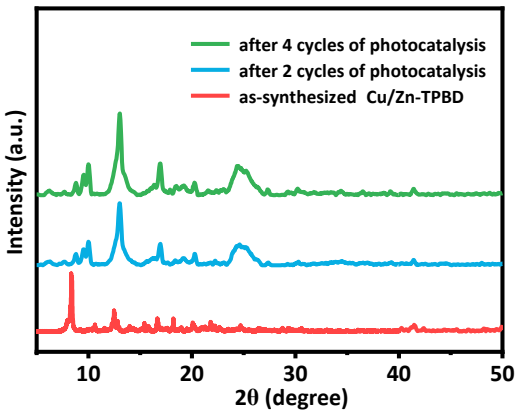

Figure S28. PXRD pattern of Cu/Zn-TPBD and Cu/Zn-TPBD after four times catalytic cycle reaction. Compared with pristine photocatalysts, the PXRD peaks of Cu/Zn-TPBD became narrower after four catalytic recycling, which might be attributed to particle agglomeration leading to an increase in crystallite size, reducing the overall surface area.

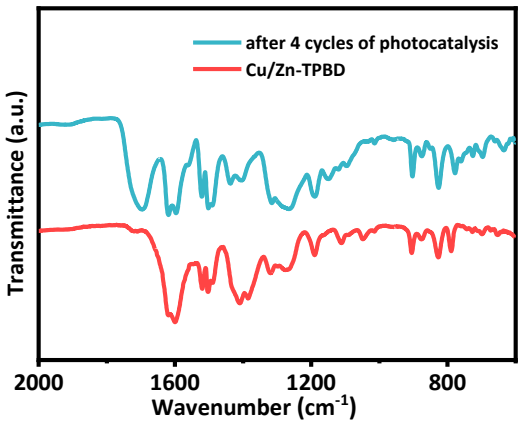

Figure S29. FTIR spectra of pristine Cu/Zn-TPBD and Cu/Zn-TPBD after four times catalytic cycle reaction. It should be noted that, the FTIR spectra of Cu/Zn-TPBD exhibit consistent characteristic peaks before and after catalytic cycles, with only a new signal emerging at approximately 1720 cm^{-1} after recycling process. This peak likely originates from minor structural adjustments within the Cu/Zn-TPBD framework, caused by its prolonged exposure to ROS and the concomitant introduction of carbonyl groups.

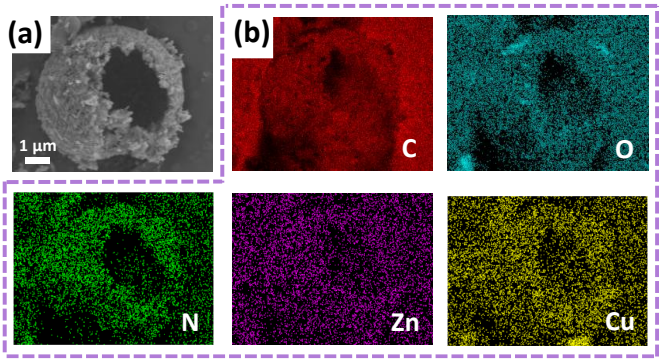

Figure S30. (a) SEM and (b) EDX mapping images of Cu/Zn-TPBD after four times catalytic cycle reaction.

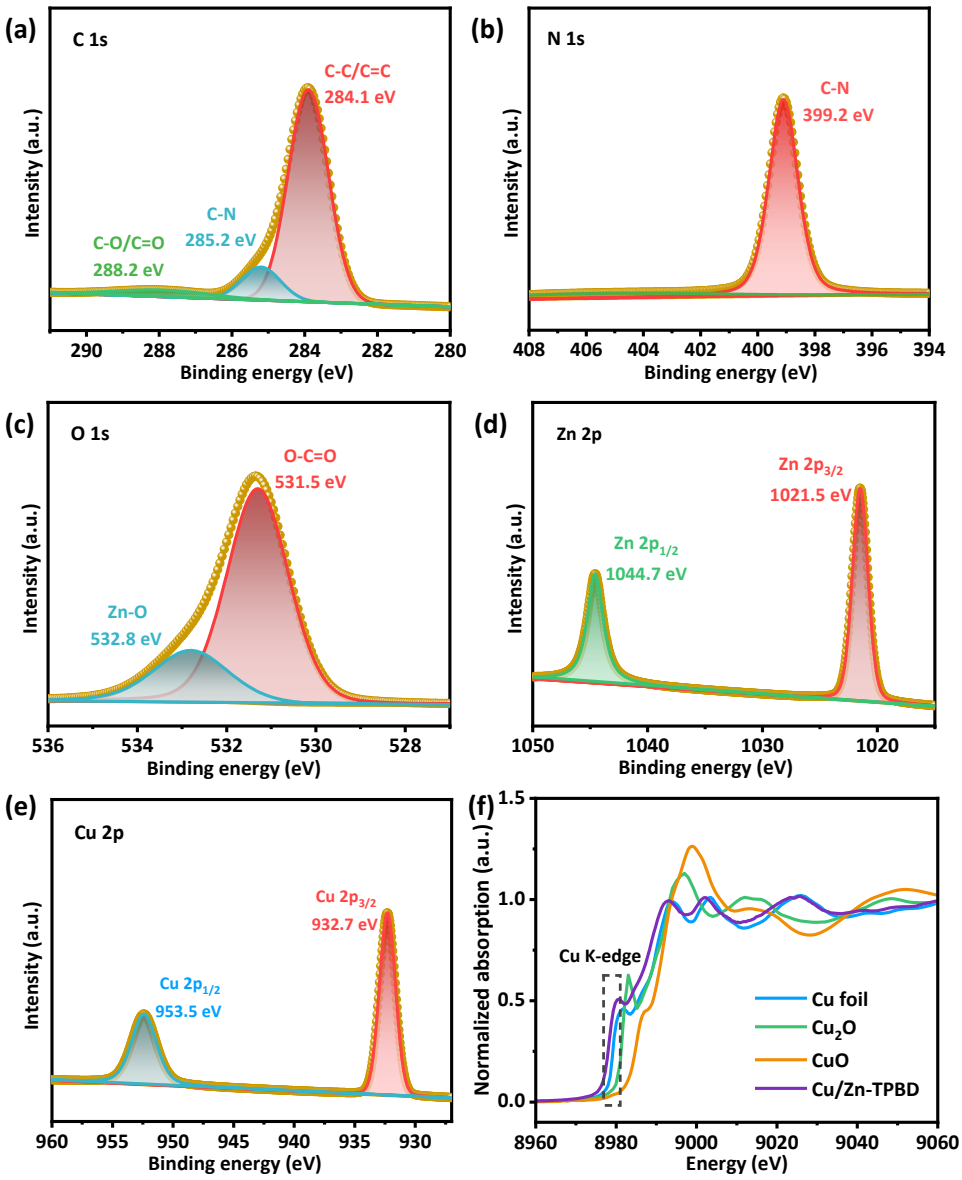

Figure S31. (a) C 1s spectrum, (b) N 1s spectrum, (c) O 1s spectrum, (d) Zn 2p spectrum, (e) Cu 2p spectrum and (f) XANES K-edge spectra of Cu/Zn-TPBD after four times catalytic cycle reaction.

Quinoline (2a)

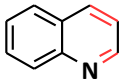

^{1}H NMR (400 MHz, $CDCl_3$): δ 8.92 (dd, *J* = 4.2, 1.8 Hz, 1H), 8.15 (ddq, *J* = 17.8, 8.6, 0.9 Hz, 2H), 7.83 (dd, *J* = 8.2, 1.5 Hz, 1H), 7.71 (ddd, *J* = 8.4, 6.9, 1.5 Hz, 1H), 7.54 (ddd, *J* = 8.1, 6.8, 1.4 Hz, 1H), 7.40 (dd, *J* = 8.3, 4.2 Hz, 1H). ^{13}C NMR (151 MHz, $CDCl_3$): δ 150.45, 148.33, 136.07, 129.50, 129.47, 128.31, 127.80, 126.56, 121.10.

6-methoxyquinoline (2b)

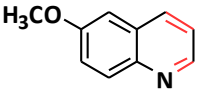

^{1}H NMR (400 MHz, $CDCl_3$): δ 8.80 – 8.73 (m, 1H), 8.06 – 8.02 (m, 1H), 8.00 (d, *J* = 9.3 Hz, 1H), 7.36 (ddd, *J* = 10.9, 8.7, 3.5 Hz, 2H), 7.07 (d, *J* = 2.8 Hz, 1H), 3.92 (s, 3H). ^{13}C NMR (151 MHz, $CDCl_3$): δ 157.71, 147.94, 144.46, 134.71, 130.87, 129.27, 122.22, 121.32, 105.10, 55.50.

6-Chloroquinoline (2c)

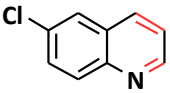

^{1}H NMR (400 MHz, $CDCl_3$): δ 8.88 (dd, *J* = 4.2, 1.8 Hz, 1H), 8.06 – 7.99 (m, 2H), 7.76 (d, *J* = 2.4 Hz, 1H), 7.62 (dd, *J* = 9.1, 2.5 Hz, 1H), 7.39 (dd, *J* = 8.5, 4.3 Hz, 1H). ^{13}C NMR (151 MHz, $CDCl_3$): δ 150.61, 146.64, 135.14, 132.30, 131.12, 130.42, 128.84, 126.42, 121.92.

6-methylquinoline (2d)

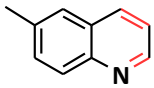

^{1}H NMR (400 MHz, $CDCl_3$): δ 8.90 – 8.80 (m, 1H), 8.09 – 8.03 (m, 1H), 8.00 (d, *J* = 8.6 Hz, 1H), 7.59 – 7.50 (m, 2H), 7.35 (dd, *J* = 8.3, 4.2 Hz, 1H), 2.53 (s, *J* = 1.0 Hz, 3H). ^{13}C NMR (151 MHz, $CDCl_3$): δ 149.51, 146.90, 136.34, 135.31, 131.70, 129.11, 128.29, 126.55, 121.03, 21.53.

Quinaldine (2e)

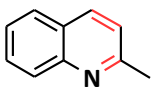

^{1}H NMR (400 MHz, $CDCl_3$): δ 8.04 (td, *J* = 8.5, 1.0 Hz, 2H), 7.77 (dd, *J* = 8.2, 1.4 Hz, 1H), 7.68 (ddd, *J* = 8.5, 6.9, 1.6 Hz, 1H), 7.48 (ddd, *J* = 8.3, 6.9, 1.4 Hz, 1H), 7.28 (d, *J* = 8.4 Hz, 1H), 2.74 (s, 3H). ^{13}C NMR (151 MHz, $CDCl_3$): δ 158.98, 147.89, 136.12, 129.38, 128.65, 127.46, 126.47, 125.63, 121.97, 77.20, 25.38.

2-methylquinoline-8-carboxylic acid (2f)

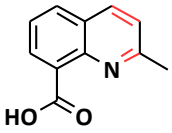

^{1}H NMR (400 MHz, $CDCl_3$): δ 8.61 (dd, *J* = 7.5, 1.4 Hz, 1H), 8.22 (d, *J* = 8.4 Hz, 1H), 7.97 (dd, *J* = 8.1, 1.5 Hz, 1H), 7.65 – 7.47 (m, 1H), 7.40 (d, *J* = 8.5 Hz, 1H), 2.75 (s, 3H). ^{13}C NMR (151 MHz, $CDCl_3$): δ 167.46, 158.61, 144.75, 138.53, 134.86, 132.66, 126.31, 126.26, 123.83, 122.69, 24.70.

1-methyl-isoquinoline (2g)

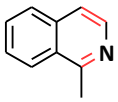

^{1}H NMR (400 MHz, $CDCl_3$): δ 8.39 (d, *J* = 5.8 Hz, 1H), 8.11 (dq, *J* = 8.5, 1.0 Hz, 1H), 7.81 (dt, *J* = 8.4, 1.0 Hz, 1H), 7.68 (ddd, *J* = 8.2, 6.9, 1.4 Hz, 1H), 7.59 (ddd, *J* = 8.4, 6.9, 1.4 Hz, 1H), 7.51 (d, *J* = 5.8 Hz, 1H), 2.97 (s, 3H). ^{13}C NMR (151 MHz, $CDCl_3$): δ 158.61, 141.81, 135.91, 129.94, 127.52, 127.21, 127.04, 125.64, 119.29, 22.42.

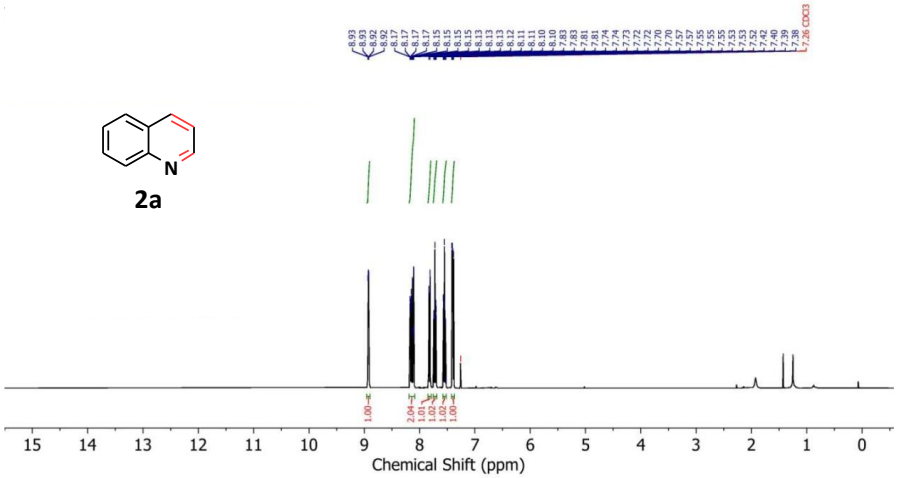

Figure S32. ^{1}H NMR spectrum (400 MHz, $CDCl_3$) of **2a**.

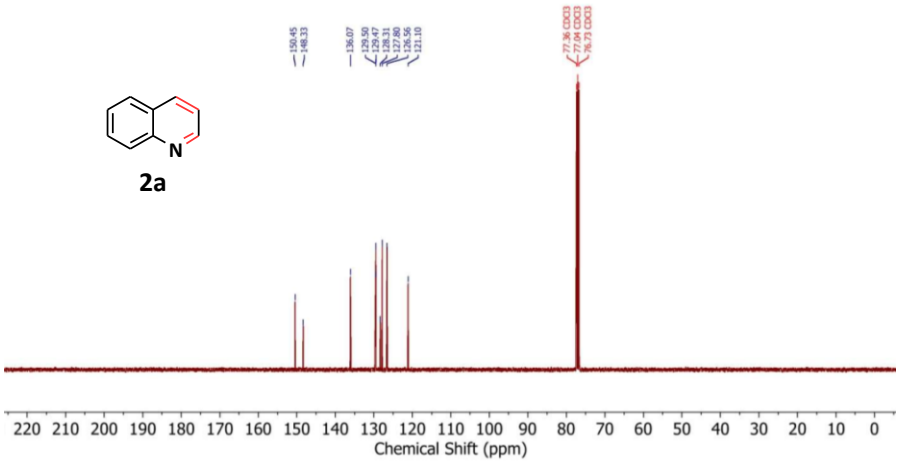

Figure S33. ^{13}C NMR spectrum (151 MHz, $CDCl_3$) of **2a**.

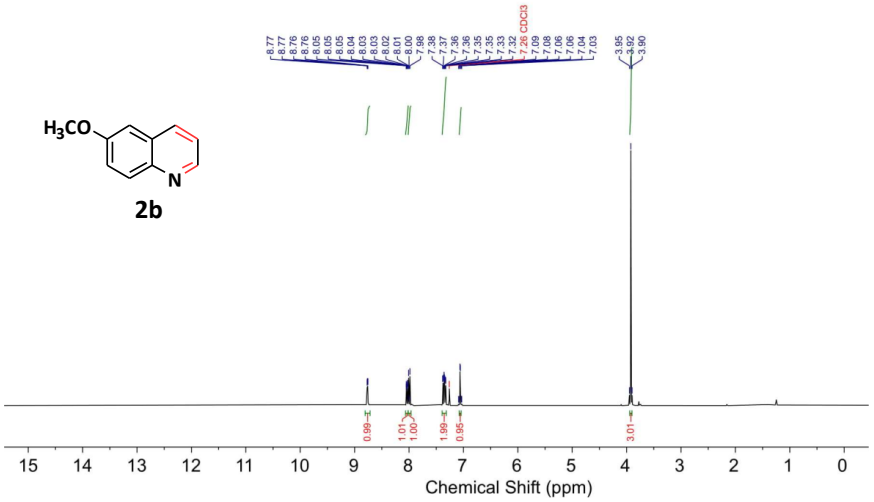

Figure S34. ^{1}H NMR spectrum (400 MHz, $CDCl_3$) of **2b**.

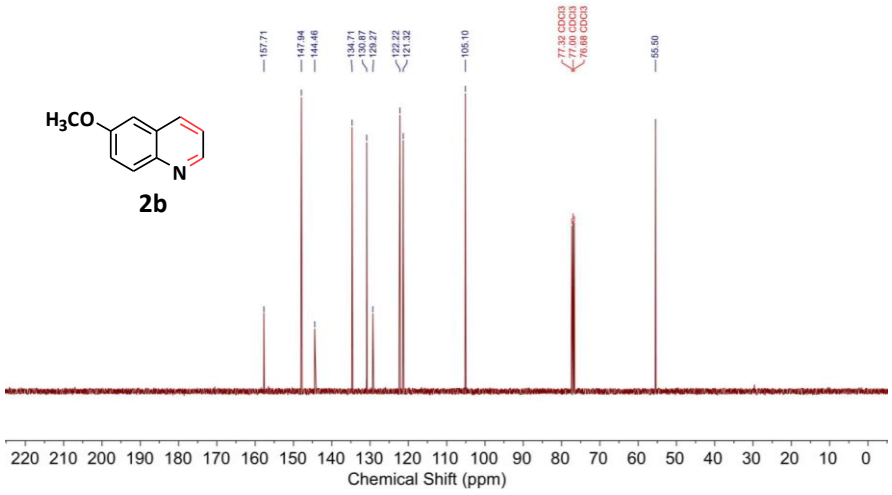

Figure S35. ^{13}C NMR spectrum (151 MHz, $CDCl_3$) of **2b**.

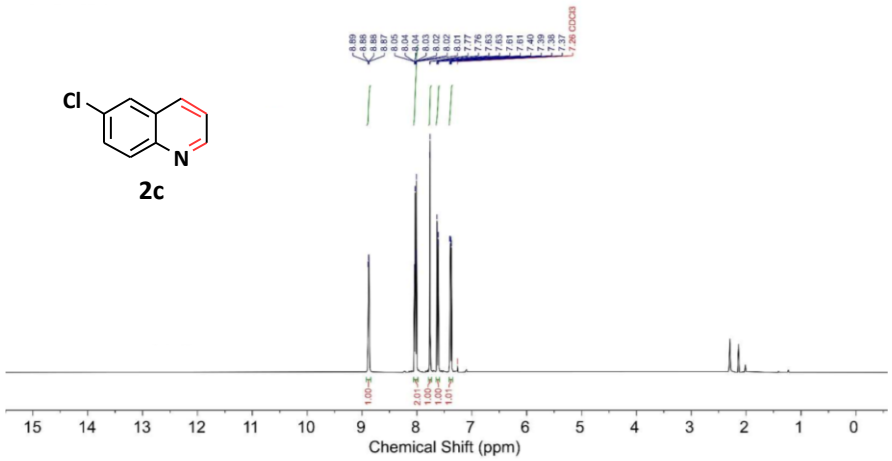

Figure S36. ^{1}H NMR spectrum (400 MHz, $CDCl_3$) of **2c**.

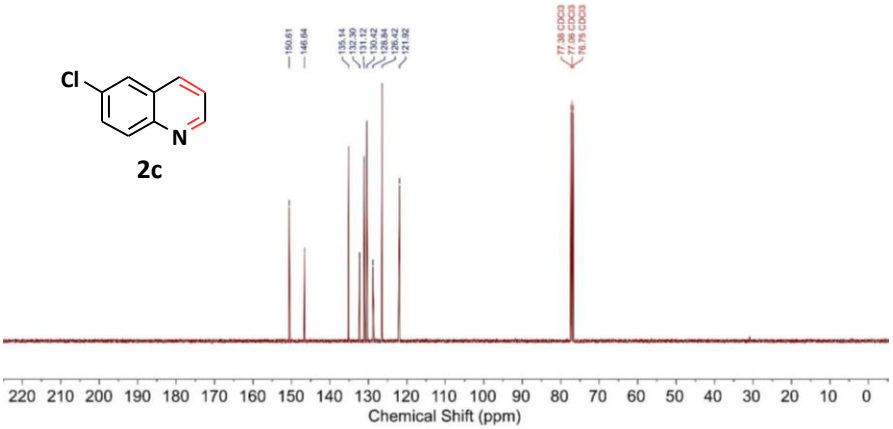

Figure S37. ^{13}C NMR spectrum (151 MHz, $CDCl_3$) of **2c**.

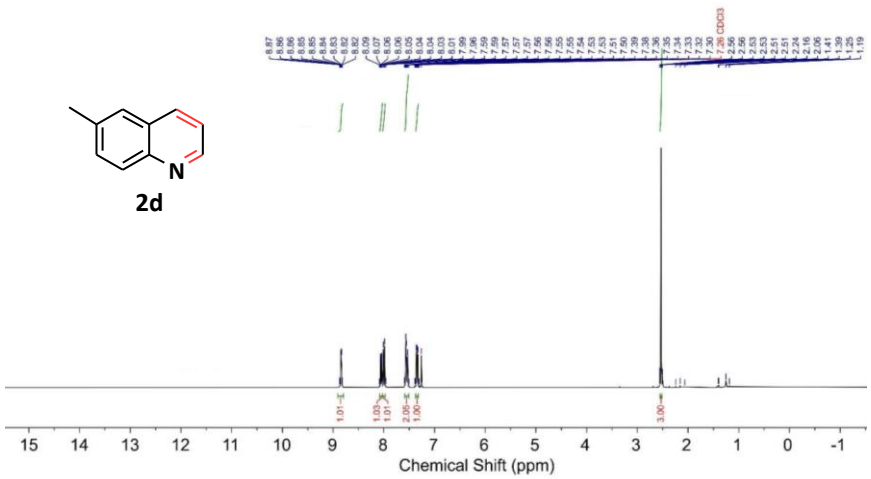

Figure S38. ^{1}H NMR spectrum (400 MHz, $CDCl_3$) of **2d**.

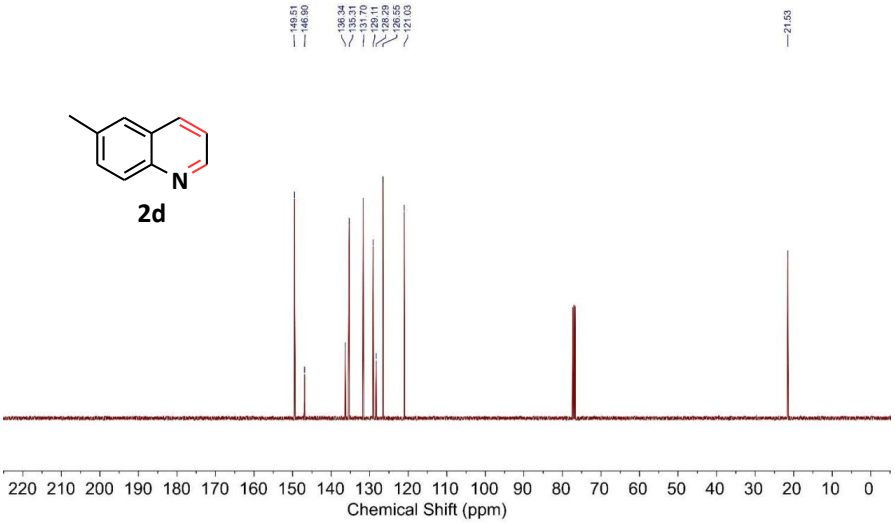

Figure S39. ^{13}C NMR spectrum (151 MHz, $CDCl_3$) of **2d**.

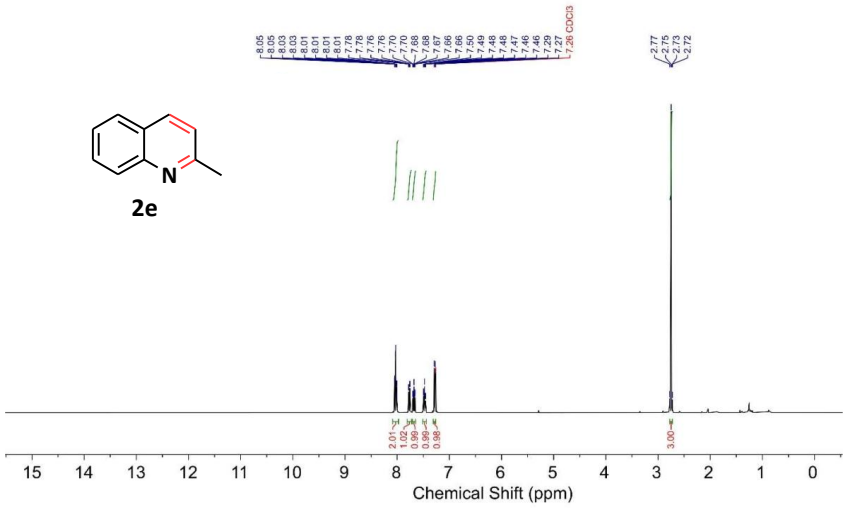

Figure S40. ^{1}H NMR spectrum (400 MHz, $CDCl_3$) of **2e**.

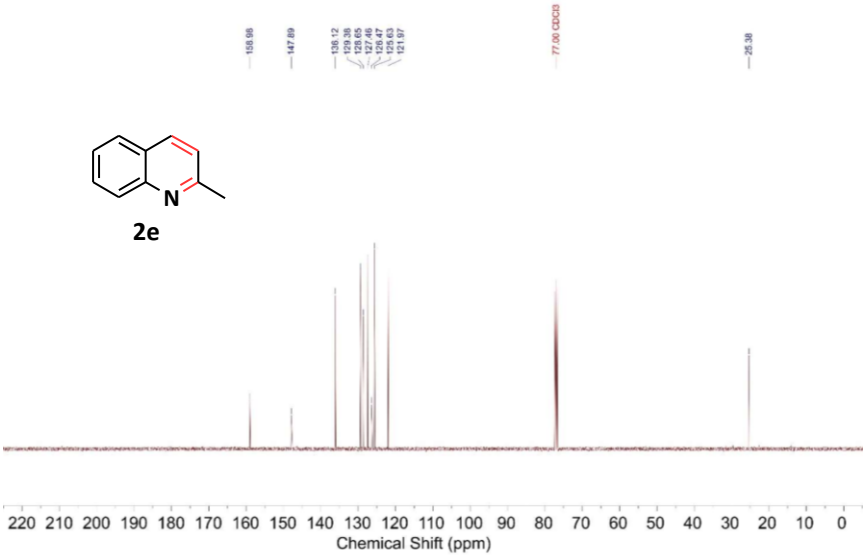

Figure S41. ^{13}C NMR spectrum (151 MHz, $CDCl_3$) of **2e**.

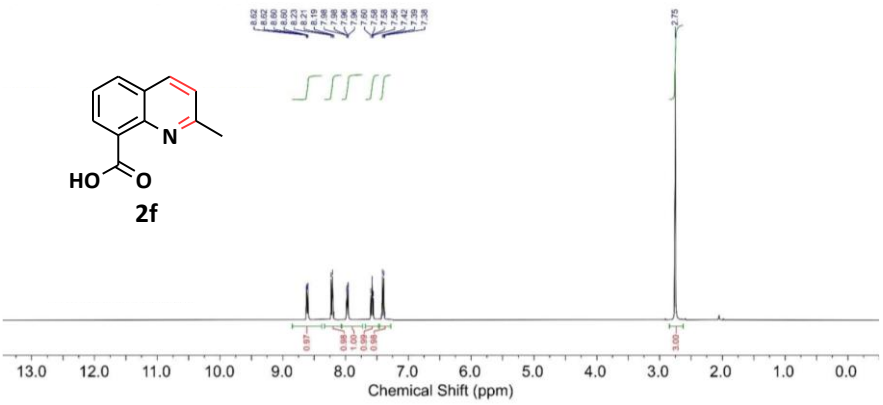

Figure S42. ^{1}H NMR spectrum (400 MHz, $CDCl_3$) of **2f**.

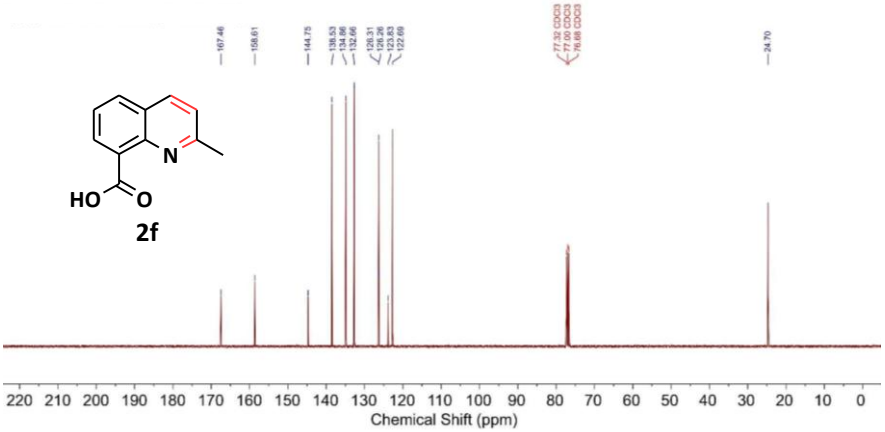

Figure S43. ^{13}C NMR spectrum (151 MHz, $CDCl_3$) of **2f**.

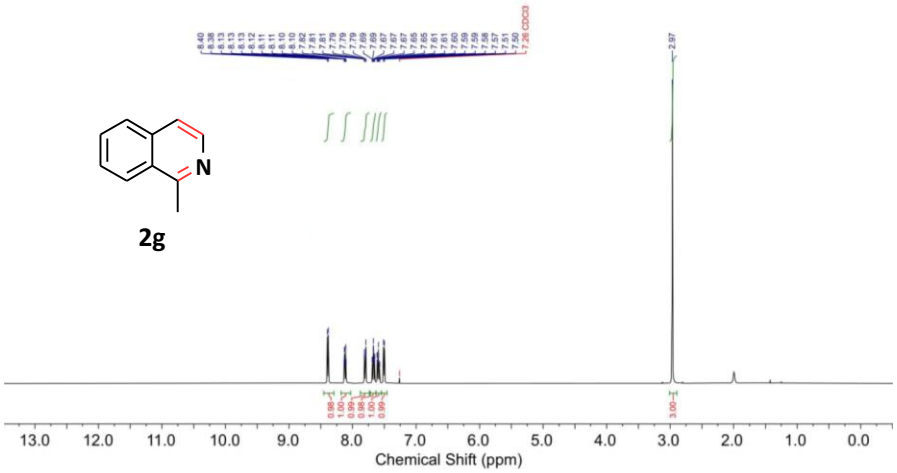

Figure S44. ^{1}H NMR spectrum (400 MHz, $CDCl_3$) of **2g**.

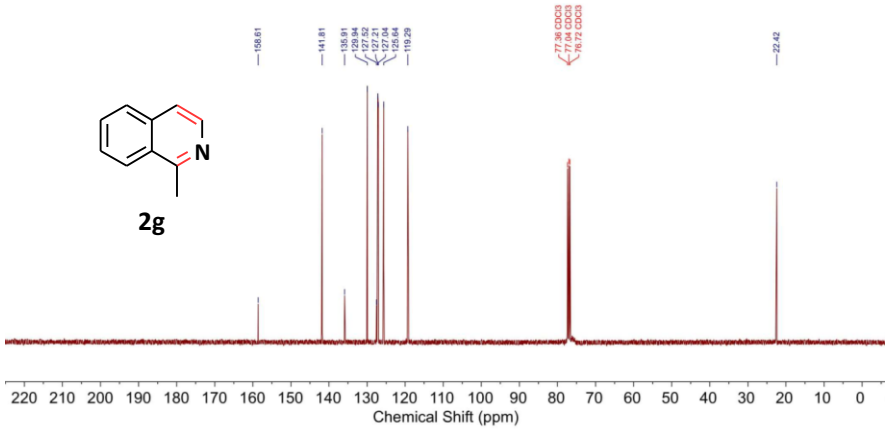

Figure S45. ^{13}C NMR spectrum (151 MHz, $CDCl_3$) of **2g**.

4. References

S1. L. X. Hou, X. Jing, H. L. Huang and C. Y. Duan, *ACS Appl. Mater. Interfaces*, 2022, **14**, 15307–15316.

S2. L. X. Hou, X. Jing, H. L. Huang and C. Y. Duan, *Chem. Commun.*, 2023, **59**, 3407–3410.

S3. W. J. Shi, T. H. Shen, C. K. Xing, K. Sun, Q. H. Yan, W. Z. Niu, X. Yang, J. J. Li, C. Y. Wei, R. J. Wang, S. Q. Fu, Y. Yang, L. Y. Xue, J. F. Chen, S. W. Cui, X. Y. Hu, K. Xie, X. Xu, S. Duan, Y. F. Xu and B. Zhang, *Science*, 2025, **387**, 791–796.

S4. I. Kim, G. B. Lee, S. Kim, H. D. Jung, J. Y. Kim, T. Lee, H. Choi, J. Jo, G. Kang, S. H. Oh, W. Kwon, D. Hong, H. G. Kim, Y. Lee, U. Kim, H. Kim, M. Kim, S. Back, J. Park, Y. C. Joo and D. H. Nam, *Nat. Catal.*, 2025, **8**, 697–713.

S5. L. J. Liu, J. Y. Lu, Y. H. Yang, W. Ruettinger, X. H. Gao, M. Wang, H. Lou, Z. D. Wang, Y. F. Liu, X. Tao, L. N. Li, Y. Wang, H. J. Li, H. Zhou, C. T. Wang, Q. S. Luo, H. X. Wu, K. D. Zhang, J. B. Ma, X. M. Cao, L. Wang and F. S. Xiao, *Science,* 2024, **383**, 94–101.

S6. B. Ravel and M. Newville, *J. Synchrotron Radiat.*, 2005, **12**, 537–541.